

- (4) P. Biereichel, B. Gustafsson, G. Raffi, 1983, The New Data Acquisition System for ESO Instrumentation, *The Messenger* **34**, 35.
- (5) H. Dekker and S. D'Odorico, 1984, First QSO Spectra with EFOSC, *The Messenger* **37**, 7.

Table 1. Available filters and standard apertures.

In the filter wheel, up to 11 filters may be mounted. The aperture wheel will hold up to 10 standard or special (multi-hole) aperture plates; one position is reserved for an inclined mirror for use with the slit viewer, one position must be free for direct imaging. The twin slits are primarily intended to be used with the cross-dispersed grism.

Filters

A set of redshifted H α and [OIII] interference filters:

Redshift	Centre wavelength/FWHM	
km/sec	[OIII]	H α
0	5010/66/130	6562/61/142
3000	5060/56	6634/70
6000	5111/55	6693/94
9000	5162/63	6766/68
12000	5211/60	6832/74
15000	5261/54	
18000	5313/55	6956/64
21000	5354/64	7018/64

A set of U, B, V, R filters.

A set of Gunn G, R, I, Z filters.

Standard aperture plates:

Slits with a length of 3.6':
.5", .75", 1", 1.5", 2", 2.5", 3", 5", 10".

Twin slits 50" apart, each 5" long:
1", 1.5", 2", 3", 6".

Abundances in LINERs

L. Binette, ESO

Introduction

Ionized gas can be detected in the nucleus of most bright galaxies as shown by the recent surveys of Keel (1), Stauffer (2), Phillips et al. (3) and Heckman et al. (4). In fact, Keel detected nuclear emission in all the spiral galaxies (not edge-on) of his magnitude-limited complete sample. Apart from demonstrating that nuclear emission is a common phenomenon, these surveys also showed that the emission can be broadly divided into three classes: those that bear many similarities with spiral arm HII regions and for which young OB type stars are the likely excitation mechanism; secondly, those that are characterized by low excitation lines such as [NII], [OII], [SII] and [OI], which have been termed LINERs (for Low Ionization Nuclear Emission Regions) by Heckman (5), and, finally, the higher excitation (and rarer) Seyferts galaxies which often reveal an important UV continuum excess. The recognized excitation mechanism for Seyferts is photoionization by a non-stellar object.

In the case of LINERs, the excitation mechanism is still debatable. Because of the predominance of low ionization species in the spectra, excitation by shocks appeared promising at first and has been proposed by Heckman. However,

recent work by Ferland and Netzer (6), Halpern and Steiner (7) and Keel (8) shows that photoionization by non-thermal UV spectra more easily reproduces the spectral features of LINERs; the latter are also shown to form a natural sequence with Seyferts or Quasars with the ionization parameter as the connecting variable. In support of this, properties like broad Balmer lines or nuclear X-ray flux which are often associated with Seyferts, are also observed in a substantial fraction of LINERs. Although photoionization is adopted in the analysis that follows, the possibility that both mechanisms may be operating to different degrees in different objects cannot be ruled out (Aldrovandi and Contini (9)).

We here present a project summary on LINERs for which two types of results are available at this stage: first, new diagrams of emission line ratios which reveal tighter correlations when homogeneous data are used, second, a new grid of photoionization calculations which aim at analysing the sensitivity to input parameters like optical thickness, hardness of the ionizing spectrum and distribution of the gas. It is concluded that abundances are more uniform (and solar) than previous work suggested.

New Diagnostic Diagrams for LINERs

Although photoionization models have proved successful in reproducing various correlations in selected diagnostic diagrams, the scatter of the data remained nevertheless substantial. From trying out new combinations of line ratios, however, it has become apparent that this scatter can be significantly reduced if one defines diagrams which are optimized for the type of spectrum that characterises LINERs; as a by-product, these new diagrams also give more compelling evidence in favour of photoionization. For example, there are many advantages in replacing the much in vogue OII/OIII axis which represents the excitation of the gas, by OI/OIII, an equivalent excitation index. (Obviously, this is only possible for classes of objects like LINERs which present a significant [OI] flux). While the previously used OIII/H β versus OII/OIII diagram is significantly affected by interstellar extinction or by collisional deexcitation due to high densities, the new diagram proposed in Fig. 1 is quite insensitive to these effects. In fact, the dispersion introduced in Figs. 1 and 2 due to reddening is quite small because the reddening correction (represented by the arrow normalized to E(B-V) = 0.66) runs in about the same direction as the correlation shown by the objects. Similar considerations apply to the effect on the line ratios of collisional deexcitation. For instance, the dispersion introduced by varying the densities is no more than 0.24 dex if these are below $4.0 \times 10^5 \text{ cm}^{-3}$ (this result is born out of computations of models such as those described below). Another factor favouring Fig. 1 is that it is quite insensitive to geometrical parameters defining the gas distribution as has been shown using spatially "integrated" models. Unfortunately, one parameter – optical thickness – could pose a serious problem for any diagram involving [OI] but, as it turns out, the ionized condensations appear to be optically thick at least in the majority of the objects. This is indicated by the scatter which should otherwise be larger than observed in Fig. 1. The possibility of optical thinness is further discussed in Binette (10).

A set of spectral data on LINERs larger than available to Ferland and Netzer or Halpern and Steiner is plotted in Figs. 1 and 2; it includes data from both Keel (8) and Stauffer (11). (A few ellipticals have been added by Keel to the subset). These data are represented by squares except for the higher excitation objects of Stauffer for which diamonds are used. These latter objects would not strictly be classified as LINERs if Heckman's criterion concerning the relative strength of [OIII] is

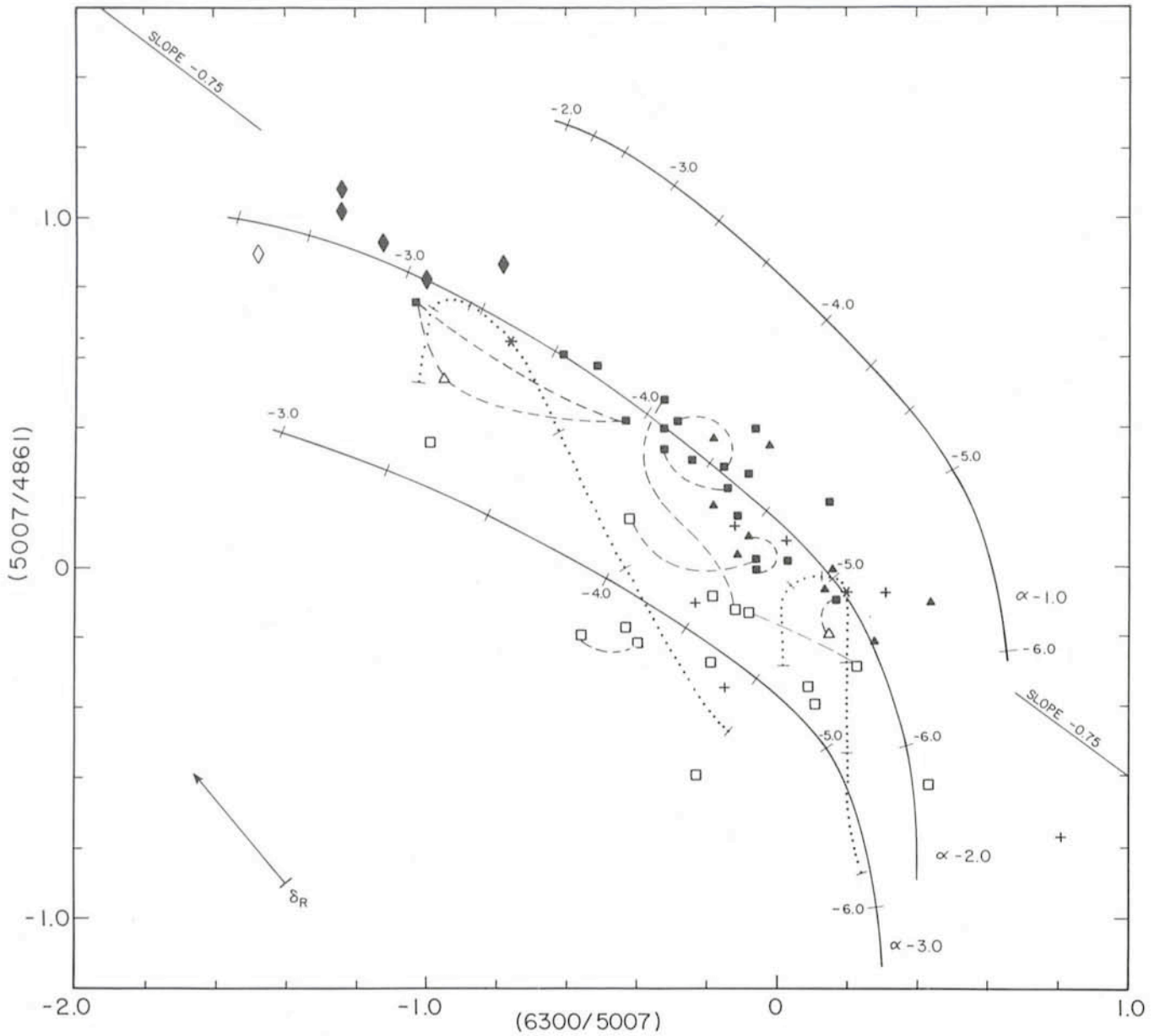


Fig. 1: $[OIII]/H\beta$ versus $[OI]/[OIII]$ diagram for models; for the sample galaxies, the ordinate is $[OIII]/(H\alpha/3)$. Squares represent objects from Stauffer (11) and Keel (8). Diamonds distinguish the higher excitation objects from Stauffer. Triangles are allocated to the sample of Heckman et al. (4) as listed in Ferland and Netzer (6). Open figures characterize objects which are more than 0.17 dex below the straight line (or envelope) of slope -0.75 . Broken lines join multiple measurements of the same object. Continuous lines represent the locus of "integrated" models (with $\alpha = -1, -2, -3$) while asterisks and dotted lines refer to individual calculations at various abundances (here $\alpha = -2$).

invoked. On the other hand, one can doubt of its relevance in the context of surveys where unnecessary preselection could hide meaningful trends across classes. One must also bear in mind that Stauffer discovered these objects following the same systematic procedure as for the LINERs and even though they could be labelled Seyferts, they are at least of a very underluminous sort and quite homogeneous in spectral properties. This is seen in Figs. 1 and 2 where diamonds appear simply as an extension to LINERs, which suggests that these objects represent a difference in degree and not in class. However, this is a point requiring further confirmation since the statistics are rather limited. Finally, to complete the data base, the LINERs from the list given in Ferland and Netzer (6) that correspond to the magnitude-limited survey of Heckman et al. (4) are included and represented by the triangles. It should be noted that no correction for reddening has been applied to the data shown and that the $H\beta$ flux used in ordinate of Fig. 1 was always derived from the $H\alpha$ measurement, using: $H\beta = H\alpha/3.0$.

One of the most significant results from Fig. 1 is that three quarters of the objects taken from *complete magnitude-limited samples* can be contained in a linear band 0.3 dex wide only (the range in $OI/OIII$ covers 1.7 dex). Inspection of Fig. 1 suggests that the objects' distribution is characterized by an "upper envelope" towards which the objects tend to concentrate. The latter is empirically defined as a straight line of slope -0.75 and intercept $(0.0, 0.2)$. Filled symbols in both figures correspond to objects which fall within 0.17 dex of the line and, conversely, the open symbols are assigned to the more distant objects below the envelope. It is remarkable, and certainly not fortuitous, that most survey objects are confined to a relatively narrow band. This shows that a sample of emission galaxies not biased towards high luminosity emission line objects (as is the case for objective prism detection surveys, for example) has relatively homogeneous spectral properties. Incidentally, LINERs from ill-defined samples such as those listed in Ferland and Netzer (which complements the subset of Heck-

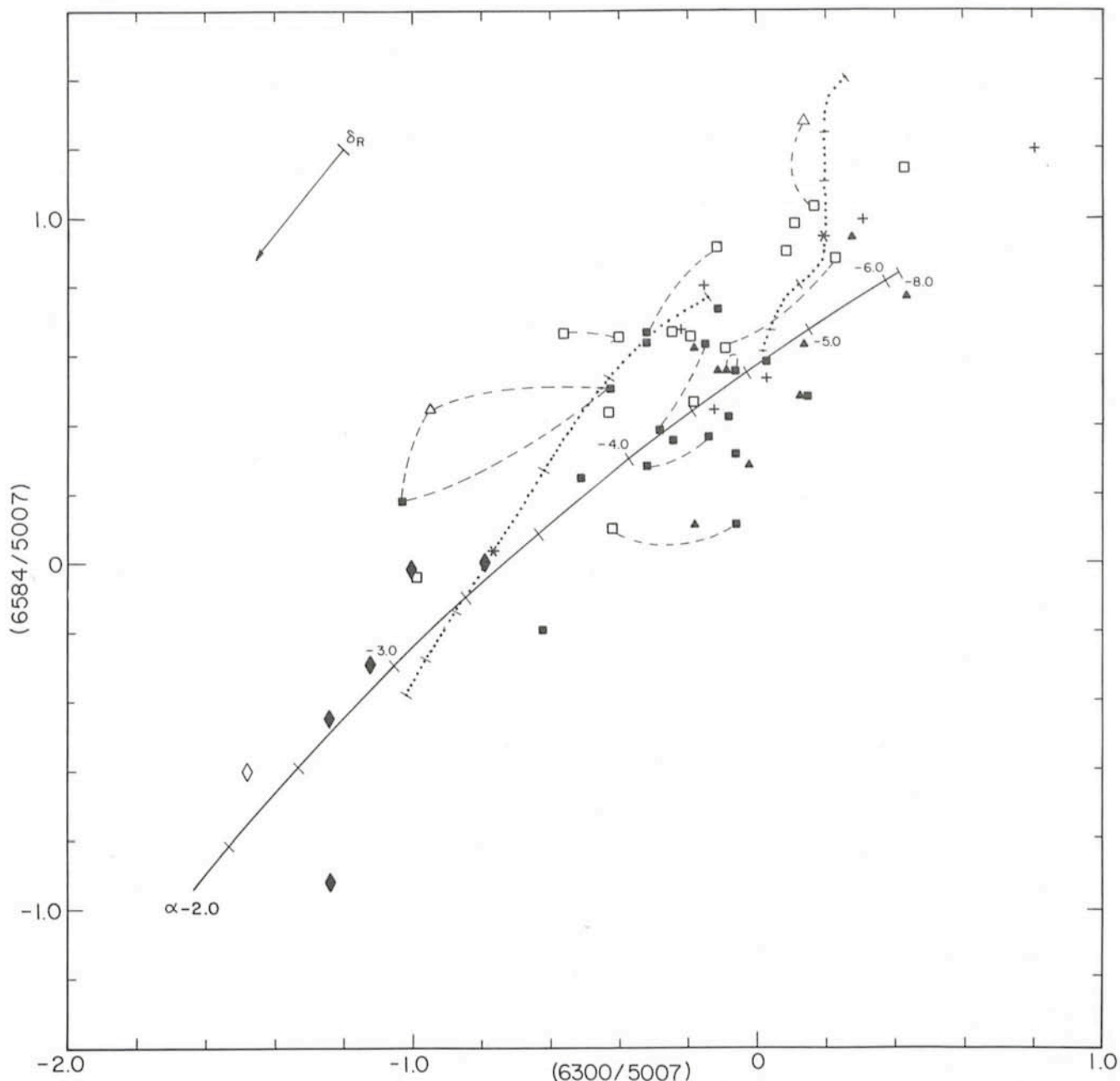


Fig. 2: $[NII]/[OIII]$ versus $[OI]/[OIII]$ diagram. Symbols have the same meaning as in Fig. 1.

man et al.), if included, considerably increase the scatter in the diagrams. They also have a clear tendency to appear significantly below the envelope. The explanation for this as well as for the particular position of open-symbol objects is probably that the clouds are optically thin or, alternatively, that these objects have superimposed nuclear HII regions besides the LINER phenomenon, as discussed in Binette (10). Metallicity variations are apparently not relevant here since a correlation exists between line luminosity of an object and its distance in Fig. 1 from the upper envelope. For this reason, we will concentrate on filled-symbol objects in the following discussion on abundances.

Photoionization Calculations

The smaller scatter in the new diagrams can be used to set some interesting limits on the variations of abundances from object to object. To determine, on the other hand, what these

abundances are relative to hydrogen is a more difficult problem since the electronic temperature is unknown and some assumptions must be made concerning the shape of the UV ionizing spectrum which is responsible for the heating as well as for the ionization balance. As in Ferland and Netzer (6), the shape adopted here will be a power-law of index α ($F_\nu = k\nu^\alpha$) with no cutoff or extinction. The effect of varying α is illustrated in Fig. 1 for three sequences of models. The calculations were performed using the multipurpose code MAPPINGS (Binette (12)). All significant charge transfer reactions involving hydrogen or helium have been included and the effects of X-ray ionization on the ionic and thermal balance have been fully accounted for.

Previous photoionization calculations assumed only discrete values of the ionization parameter U (which expresses the density of impinging ionizing photons relative to the cloud's density). The present calculations on the other hand (the loci of which are shown as continuous lines) were

obtained by summing up the contributions of clouds at different distances from the ionizing source. This is justified since the emission in LINERs is spatially resolved and known to cover hundreds of parsecs in diameter. Because most spectrophotometric data were obtained through circular or square apertures, the spectrum likely represents a mixture of high and low ionization lines emitted at different radii, an effect taken into account in the present models. The filling factor (or number) of ionized clouds has been assumed to decrease exponentially with distance from a centrally located ionizing source; the cloud density was fixed at 400 cm^{-3} . It was assumed that the clouds were individually optically thick but because the observed filling factor is very small, the covering factor of (intervening) clouds was always considered negligible. This method, described in more detail in ref. 10, is obviously applicable to the gas-limited geometries thought to prevail in LINERs (cf. Keel (1)) rather than to radiation-limited geometries. Adopting a spherical distribution of clouds, the resulting models will hereafter be labelled "integrated". They are characterized by an effective U_e which is simply a weighted average of the ionization parameter. Fiducial marks along the continuous lines indicate successive values of $\text{Log } U_e$ with a step of -0.3 between integer values (e. g. $-3.0, -3.3, -3.6 \dots$). In order to show the relative position of "non-integrated" models, calculations at values of $\text{Log } U$ of -3.0 and -3.6 are represented by asterisks (left and right respectively). It is clear from Fig. 1 that integrated or discrete U sequences overlap quite well but with a systematic shift in the value of U between the two sequences.

The two dotted curves in Figs. 1 and 2 show the effect of varying the abundances (the asterisks are actually part of these curves) and the fiducial marks from left to right correspond to successive increases by factor two of all elements' abundances (except He) relative to hydrogen (from $1/8$ to 8 times the reference set). The reference set of abundances was chosen to reflect the observed radial increase in metallicity in spirals as determined by supernova remnants' and HII regions' abundance analysis. Its main characteristics (by number) are as follows: $\text{He}/\text{H} = 0.10$, $\text{O}/\text{H} = 0.001$, $\text{O}/\text{N} = 3.0$ and $\text{O}/\text{S} = 45$ (for comparison, solar abundances would give: 0.085 , 0.0008 , 8 and 41 respectively). A mild depletion of the refractory elements C, Mg, Si has been allowed for.

In Figs. 1 and 2, the index $\alpha = -2.0$ appears the best choice for the objects as a whole and is adopted. In support of this we

note that the observed upper envelope in Fig. 1 is probably a consequence of a moderately steep ionizing spectrum since, as shown by the dotted lines, varying abundances only populate a region below the maximum in $\text{OIII}/\text{H}\beta$ that occurs around solar values. It must be emphasized that with the flatter indices used in previous work, this turnaround in the $[\text{OIII}]$ intensity would only occur at very high metallicity so that with reasonable abundances $[\text{OIII}]$ is then simply proportional to metallicity. This could explain how previous calculations favoured anomalous abundances of 0.3 solar since otherwise the majority of objects were found to be below the locus of their solar abundances' models.

As for the metallicity of the nuclear interstellar medium, the two dotted lines in Fig. 1 show the filled-symbol objects to be consistent with abundances that are roughly solar with variations in these probably confined to between solar and three times solar. This range of variations is smaller than in Keel (8) who derived an $(\text{N}+\text{O})$ abundance index that ranges from 0.88 to 4.7 times solar. Concerning nitrogen, the NII/OIII ratio of Fig. 2 scales almost linearly with the N/O abundance ratio and, therefore, the filled-symbol objects are considered consistent with variations in N/O not exceeding a factor three. It is to be noted that the determined average value ($\langle \text{N}/\text{O} \rangle = 1/3$) is definitely above solar. Since many factors, such as observational errors, differences in the ionizing spectrum or reduced optical thickness, could account for part of the scatter in the figures, it is plausible that abundances are actually even more uniform than suggested here.

References

- (1) Keel, W.C.: 1983, *Astrophys. J. Suppl.* **52**, 229.
- (2) Stauffer, J.R.: 1982, *Astrophys. J. Suppl.* **50**, 517.
- (3) Phillips, M.M., Jenkins, C.J., Dopita, M.A., Sadler, E.M. and Binette, L.: 1985, *Astrophys. J.* (submitted).
- (4) Heckman, T., Balick, B. and Crane, P.: 1980, *Astron. Astrophys. Suppl.* **40**, 295.
- (5) Heckman, T.: 1980, *Astron. Astrophys.* **87**, 152.
- (6) Ferland, G.J. and Netzer, H.: 1983, *Astrophys. J.* **264**, 105.
- (7) Halpern, J.P. and Steiner, J.E.: 1983, *Astrophys. J. Lett.* **269**, L37.
- (8) Keel, W.C.: 1983, *Astrophys. J.* **269**, 466.
- (9) Aldrovandi, S.M.V. and Contini, M.: 1983, *Astron. Astrophys.* **127**, 15.
- (10) Binette, L.: 1985, *Astron. Astrophys.* (ESO preprint 350).
- (11) Stauffer, J.R.: 1982, *Astrophys. J.* **262**, 66.
- (12) Binette, L.: 1982, Ph.D. Thesis, Australian Nat. Univ., Canberra.

Absorption Lines of Interstellar C_2 and CN Molecules

E.F. van Dishoeck, *Sterrewacht Leiden, the Netherlands, and*
 J.H. Black, *Steward Observatory, Tucson, USA*

Introduction

A considerable part of our knowledge about interstellar clouds stems from observations of their constituent molecules. In particular, diffuse interstellar clouds—i.e. clouds which do not entirely obscure the light from the stars which lie behind them—may be conveniently studied by the resonance absorption lines of the molecules superposed on the spectra of background stars. Already more than 40 years ago, the first three interstellar molecules CH , CH^+ and CN were discovered in this way at visible wavelengths. However, the next discovery of a molecule in the visible, C_2 (Souza and Lutz, 1977, *Astrophysical Journal* **216**, L 49), had to wait for the

advent of high-resolution spectrographs with detectors that are very sensitive in the red part of the spectrum. At present, one of the best instruments in the world for these observations is the ESO Coudé Echelle Spectrometer (CES). The instrument has been described previously in the *Messenger* by Enard (17, 32 and 26, 22), and its excellent performance has been demonstrated by the multitude of enthusiastic papers on CES observations in the last few issues of the *Messenger* (see e.g. Ferlet, 30, 9; Andersen et al., 34, 26).

Observations of molecules are not only interesting because they provide the abundance of the species in the interstellar